CHEMISTRY

Competitive chiral induction in a 2D molecular assembly: Intrinsic chirality versus coadsorber-induced chirality

Ting Chen,[1] Shu-Ying Li,[1,2] Dong Wang,[1,2]* Li-Jun Wan[1]*

Noncovalently introducing stereogenic information is a promising approach to embed chirality in achiral molecular systems. However, the interplay of the noncovalently introduced chirality with the intrinsic chirality of molecules or molecular aggregations has rarely been addressed. We report a competitive chiral expression of the noncovalent interaction–mediated chirality induction and the intrinsic stereogenic center–controlled chirality induction in a two-dimensional (2D) molecular assembly at the liquid/solid interface. Two enantiomorphous honeycomb networks are formed by the coassembly of an achiral 5-(benzyloxy)isophthalic acid (BIC) derivative and 1-octanol at the liquid/solid interface. The preferential formation of the globally homochiral assembly can be achieved either by using the chiral analog of 1-octanol, (S)-6-methyl-1-octanol, as a chiral coadsorber to induce chirality to the BIC assembly via noncovalent hydrogen bonding or by covalently linking a chiral center in the side chain of BIC. Both the chiral coadsorber and the intrinsically chiral BIC derivative can act as a chiral seeds to induce a preferred handedness in the assembly of the achiral BIC derivatives. Furthermore, the noncovalent interaction–mediated chirality induction can restrain or even overrule the manifestation of the intrinsic chirality of the BIC molecule and dominate the handedness of the 2D molecular coassembly. This study provides insight into the interplay of intrinsically chiral centers and external chiral coadsorbers in the chiral induction, transfer, and amplification processes of 2D molecular assembly.

INTRODUCTION

Chirality in molecular assembly has attracted considerable interest because of its relevance to applications such as enantioselective heterogeneous catalysis and chiral separation, as well as to its importance in exploring the expression of chirality in biological systems (1–4). Chiral information of a molecule can be manifested at the supramolecular level during the assembly process. Understanding the chirality induction process is of great importance in the formation of molecular assemblies and materials with precisely controllable chirality nanomaterials.

The assembly of enantiopure molecules usually gives rise to nanostructures with specific chirality (5, 6). It is one of the most widely adopted methods to form molecular assemblies with controllable chirality. Generally, chiral induction by intrinsic molecular chirality is highly efficient in molecular assembly, in which chiral molecules can act as the "chiral seed" to control the globally homochiral assembly of achiral molecules. As demonstrated in a number of molecular systems including succinic acid (4, 7), aspartic acid (8), heptahelicene (9), alkoxylated dehydrobenzo[12]annulene derivatives (10), and rod-shaped molecules with oligo(phenylene ethynylene) backbones (11, 12), a few chiral molecules (the sergeant) or a slight excess of one enantiomer (the majority) adsorb on the surface and induce a large number of achiral molecules or racemates to form an assembly with preferential chirality, following the "sergeant and soldiers principle" or "the majority rules" (13–16). One interesting phenomenon is that the addition of a small amount of structurally different enantiomers into a racemate may suppress the formation of one enantiomorphous assembly and lead to single-handed assembly (17, 18).

Noncovalently introducing stereogenic information, on the other hand, is another means of inducing a specific chirality to a two-dimensional

(2D) molecular assembly (19, 20). Adding a chiral auxiliary or using a chiral solvent can bias the majority of domains in the assembly to the same handedness and doesn't affect the assembled structure. This is because the chiral auxiliary or chiral solvent in the liquid can interact with the molecular assembly at the liquid/solid interface. On the basis of these interactions, chiral information in the chiral auxiliary or chiral solvents is transferred to the achiral molecule and guides the handedness of the molecular assembly. In a few cases, the chiral solvent environment can affect the expression of the intrinsic chirality of the building blocks in the 2D molecular assembly (21).

We have recently reported chirality control in the assembly of the achiral 5-(benzyloxy)isophthalic acid (BIC) derivatives through codeposition with the chiral analog of octanol. In the system, chiral analogs of octanol serve not only as solvents but also as coadsorbers to coassemble with the BIC derivatives at the liquid/solid interface. High-resolution scanning tunneling microscopy (STM) imaging provides direct evidence for the noncovalent interaction–mediated chirality transfer from the chiral coadsorber to the BIC derivatives. Furthermore, the coadsorber-induced chirality is of high efficiency, in which a small amount of the chiral coadsorber can induce a global chirality preference in the 2D molecular assembly (22, 23). Therefore, an intriguing question arises: What will happen if the competitive chirality induction pathways, that is, the external stereogenic center of the coadsorber and the intrinsic molecular chirality, exist simultaneously in the assembly system? Although an intramolecular chiral interplay, for example, molecules have two or more intrinsic stereogenic centers with different handedness preferences, has been reported (5, 24, 25), the effect of the chiral coadsorber on the expression of the intrinsic molecular chirality in the 2D molecular assembly has rarely been addressed. Here, we present the formation of a globally homochiral molecular assembly of BIC derivatives by introducing the external chiral analogs of 1-octanol as coadsorbers or by covalently bonding a stereogenic center to the molecule. The chemical structures of the BIC derivatives and coadsorbers are shown in Fig. 1. Codeposition of the intrinsically chiral BIC derivative and the chiral coadsorber was investigated to reveal the interplay of the noncovalently
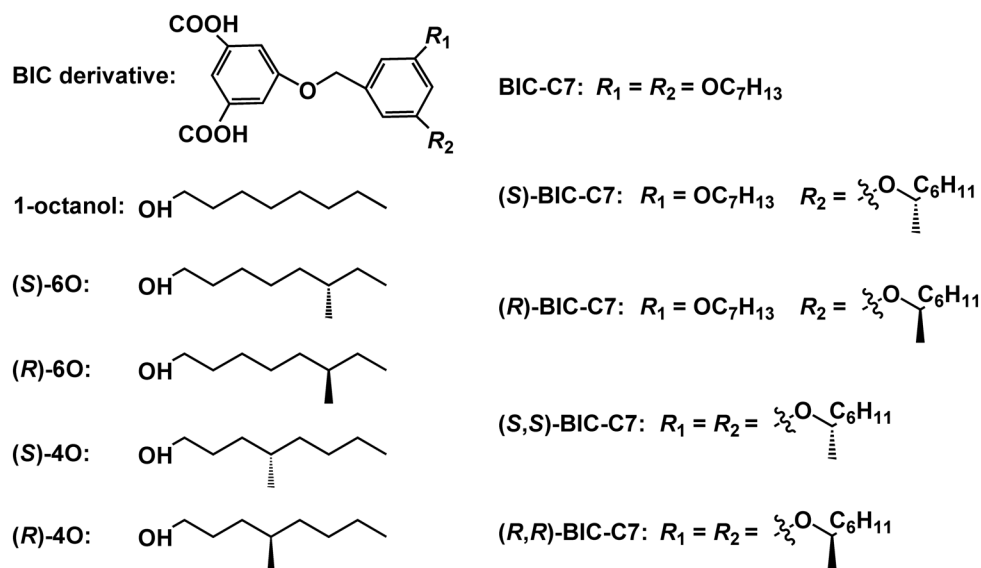
Fig. 1. Chemical structures of the BIC derivatives and 1-octanol analogs. To abbreviate a 1-octanol analog, letter "S" or "R" and a number are used to represent the spatial configuration and the position of the chiral center, respectively, and letter O represents octanol. Similarly, to abbreviate a BIC analog, one letter S or R symbolizes an S-type or R-type chiral center at one side chain.

introduced chiral information and the molecular intrinsic chirality. It is found that, in the presence of chiral coadsorbers, the expression of the intrinsic molecular chirality of the BIC derivative is suppressed at the supramolecular level, in which the chiral coadsorbers control the chirality of the 2D molecular assembly. Molecular mechanical (MM) simulation provides detailed insight into the molecular conformation changes in response to the competitive chiral induction pathways. This study reveals the effect of external noncovalently introduced chirality on chiral molecular assembly and is helpful in understanding the induction and transfer of chirality in 2D molecular assembly.

RESULTS AND DISCUSSION
Enantiomorphous honeycomb networks of the BIC-C7/1-octanol coassembly
We have investigated codeposition of BIC-C7 with 1-octanol at the liquid/solid interface and obtained two enantiomorphous honeycomb networks composed of BIC trimers (23). Figure 2 (A and B) shows high-resolution STM images of the enantiomorphous networks. BIC-C7 and the coadsorbed 1-octanol molecules can be distinguished. The unit cell parameters of the networks are $a = b = 4.8 \pm 0.1$ nm and $\alpha = 60 \pm 2°$. For clarification, a sketch of the network is superposed on each STM image, in which the thick blue sticks and the thin blue sticks represent the backbone and the side chain of the BIC-C7 molecules, respectively, and the thin yellow sticks represent the coadsorbed 1-octanol molecules. STM images, which reveal the relationship between the 2D molecular assembly and the substrate lattice, are shown in fig. S1. White arrows are used to indicate the substrate lattice directions of highly oriented pyrolytic graphite (HOPG) in Fig. 2 (A and B). It can be seen that the alkyl chains in BIC-C7 and the coadsorbed 1-octanol molecules are along the [1000] direction of the substrate. Figure S2 shows the theoretically optimized molecular models for the clockwise (CW) and counterclockwise (CCW) networks in the BIC-C7/1-octanol assembly. Multiple hydrogen bonds are formed between the carboxyl group in BIC-C7 and the hydroxyl group in 1-octanol. We investigated the codeposition of BIC-C7 with other molecules that are structurally similar to octanol, such as

octane, octylamine, octanoic acid, and n-octylbenzene, and did not observe the honeycomb network. It is suggested that the hydrogen bonding between the carboxyl group and the hydroxyl group plays an important role in the formation of the network.

According to the relative orientation of molecular backbones within the trimer, two enantiomers, CW and CCW trimers, can be resolved in Fig. 2, A and B, respectively. All trimers have the same handedness in an ordered domain, and thus, two enantiomorphous honeycomb networks corresponding to CW and CCW trimers, namely, CW and CCW networks, are present in the monolayer. Figure 2C illustrates the formation of the enantiomorphous honeycomb networks in the BIC-C7/1-octanol assembly. Statistical analysis (see details in Materials and Methods) suggests that the CW and CCW networks are presented with nearly equal percentage in the assembly. Therefore, the surface was globally racemic.

Chiral coadsorber–induced chirality in the 2D assembly of BIC-C7
When BIC-C7 was codeposited with (S)-6O or (R)-6O, similar honeycomb networks were obtained. The unit cell parameters and the orientation of the BIC-C7/(S)-6O or BIC-C7/(R)-6O coassembly are the same as those of the BIC-C7/1-octanol coassembly. Statistical analysis indicates that all networks in the BIC-C7/(S)-6O and BIC-C7/(R)-6O coassemblies are biased to CW and CCW, respectively. The results suggest that a chirality induction is achieved by the chiral coadsorber in the 2D assembly of BIC-C7. A high-resolution STM image of the BIC-C7/(S)-6O coassembly is shown in Fig. 3A. On the basis of the structural features revealed by the STM image, a molecular model of the CW network in the BIC-C7/(S)-6O coassembly was proposed and further optimized using MM simulations. The calculated molecular model is shown in Fig. 3B. The adsorption conformation of BIC-C7 is in accordance with that in the CW network of the BIC-C7/1-octanol coassembly. The methyl group at the chiral center of (S)-6O points away from the surface to minimize the steric hindrance. The scheme of the chiral induction triggered by (S)-6O in the BIC-C7 assembly is shown in Fig. 3C. The stereogenic information in the coadsorbers is efficiently transferred to BIC-C7 via noncovalent interactions and thus dictates the orientation
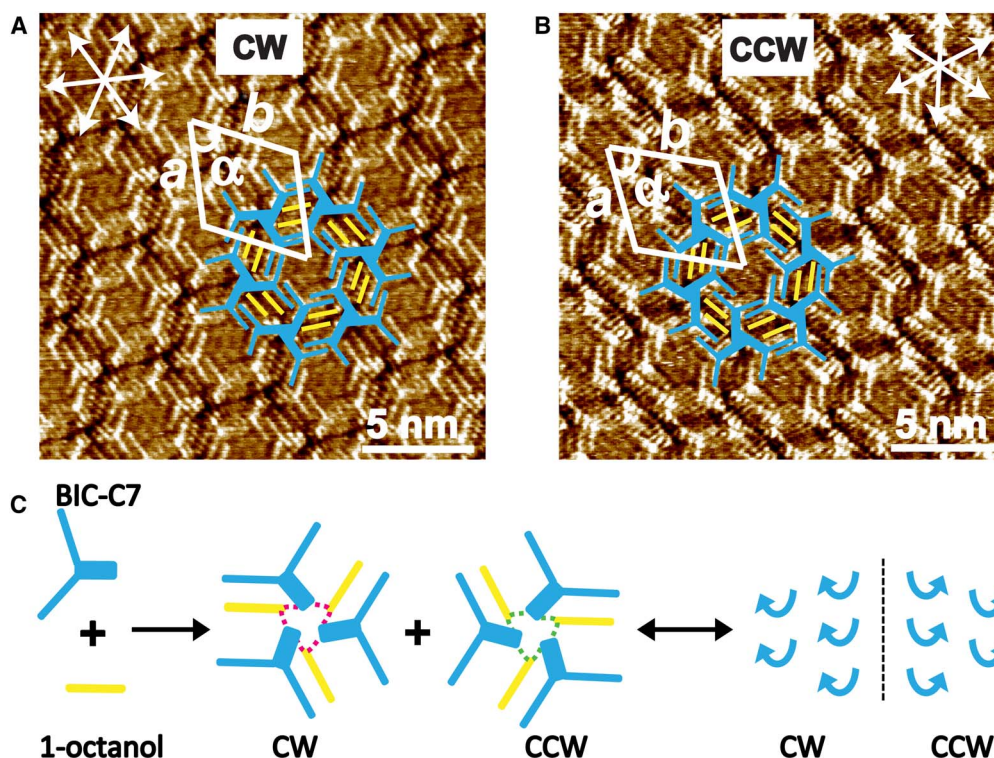
Fig. 2. Enantiomorphous honeycomb networks of the BIC-C7/1-octanol coassembly. High-resolution STM images of (**A**) the CW network and (**B**) the CCW network in the BIC-C7/1-octanol coassembly. I = 0.500 nA and V_{bias} = 0.900 V. (**C**) Formation of the enantiomorphous networks in the BIC-C7/1-octanol coassembly. The thick blue sticks, thin blue sticks, and yellow sticks represent the backbones of BIC-C7, side chains of BIC-C7, and 1-octanol molecules, respectively. The blue arrows indicate the chirality of the networks.

of the molecular backbone and subsequently determines the chirality of the molecular trimers and the 2D honeycomb networks (*22*, *23*). Figure S3 illustrates the formation of the BIC-C7/(*R*)-6O assembly.

The chiral coadsorber-induced chirality in the 2D molecular assembly is so efficient that a small amount of (*S*)-6O can be used as chiral seeds to induce the globally homochiral assembly of BIC-C7. In the experiments, BIC-C7 was dissolved in a mixed solution of 1-octanol and (*S*)-6O to a final concentration of 2.5×10^{-3} M. Then, 0.5 µl of the solution was dropped onto the HOPG surface to form the 2D molecular coassembly at the liquid/solid interface. Figure 3D shows the plot of the coverage of the CW network in the assembly versus the fraction of (*S*)-6O in the solution. It demonstrates that $78 \pm 5\%$ of the networks in the assembly is CW, although the portion of (*S*)-6O in the mixed solution of (*S*)-6O and 1-octanol is only 5 volume %. When 20 volume % of (*S*)-6O was introduced in the solution, the handedness of the BIC-C7 assembly is fully biased to CW. The result implies that (*S*)-6O is a quite effective chiral seed for chiral induction in the 2D assembly of achiral BIC-C7. Noncovalent interactions between BIC-C7 and the chiral coadsorber play important roles in the efficient chirality induction and transfer from the coadsorber to achiral BIC-C7 and the 2D molecular assembly.

Chirality induction in the coassembly of the chiral BIC-C7 analog and 1-octanol

To investigate the chiral induction via the intrinsic molecular chirality, we synthesize the chiral BIC analog by introducing one stereogenic center in the side chain. Codeposition of (*R*)-BIC-C7 or (*S*)-BIC-C7 with 1-octanol was explored. As expected, similar honeycomb networks

are formed at the liquid/solid interface. Statistical analysis reveals that all networks in the (*R*)-BIC-C7/1-octanol assembly are CCW. The result indicates that the stereogenic information in the side chain of (*R*)-BIC-C7 can be transferred to the 2D molecular assembly and dictate the chirality of the honeycomb networks. Figure 4A shows a high-resolution STM image of the (*R*)-BIC-C7/1-octanol assembly. It can be seen that the structure of the (*R*)-BIC-C7/1-octanol assembly is the same as the structures of the BIC-C7/1-octanol and BIC-C7/(*S*)-6O assemblies. Figure 4B shows the calculated molecular model of the CCW network in the (*R*)-BIC-C7/1-octanol coassembly. The methyl groups at the chiral center of (*R*)-BIC-C7 point away from the surface. This conformational preference of the chiral center in the side chain transfers along the molecular backbone and guides the orientation of the molecule within the molecular trimer unit. As a result, the handedness of the molecular trimer units and the 2D honeycomb networks is biased toward the preferred one. Figure 4C illustrates the formation of the CCW networks when (*R*)-BIC-C7 was codeposited with 1-octanol. The coassembly of (*S*)-BIC-C7 and 1-octanol is shown in fig. S4. The structure of the (*S*)-BIC-C7/1-octanol assembly is similar to the structures of the BIC-C7/1-octanol and (*R*)-BIC-C7/1-octanol assemblies, except that all networks are CW. The result further verifies that the intrinsic molecular chirality can be transferred to the 2D networks and realize chirality control in the 2D molecular assembly.

Chiral analogs with similar molecular structures can act as seeding molecules and induce a preferred chirality in the 2D molecular assembly of achiral molecules, as reported previously (*11*, *16*). Here, we found that (*S*)-BIC-C7 can serve as the chiral seed and is able to bias the assembly of achiral BIC-C7 to CW networks. No obvious preference for the CW or
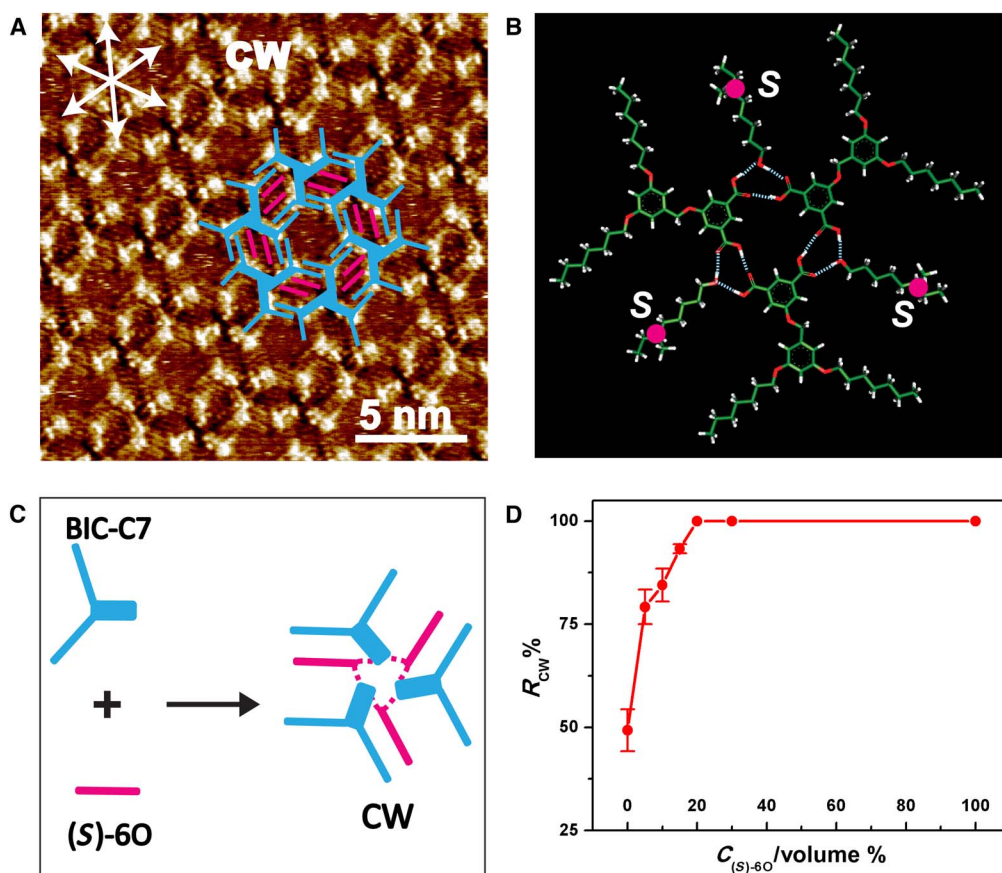
Fig. 3. Chiral induction triggered by (S)-6O in the 2D assembly of BIC-C7. (**A**) High-resolution STM image of the BIC-C7/(S)-6O coassembly. I = 0.400 nA and V_{bias} = 0.900 V. (**B**) Calculated molecular model of the trimeric unit in the BIC-C7/(S)-6O assembly. The red dot marks the (S)-type chiral center in (S)-6O. (**C**) Chiral coadsorber-induced chirality in the BIC-C7/(S)-6O assembly. The thick blue sticks, thin blue sticks, and red sticks represent the backbones of BIC-C7, side chains of BIC-C7, and coadsorbed (S)-6O molecules, respectively. (**D**) Plot of the coverage of the CW network in the assembly (R_{CW}, estimated based on the number of domains) versus the fraction of (S)-6O in a mixed solution of (S)-6O and 1-octanol.

CCW network was observed until the fraction of (S)-BIC-C7 reaches 20 mole percent (mol %), as shown in Fig. 4D. After that, the coverage of the CW network increases with the fraction of (S)-BIC-C7. When the fraction of (S)-BIC-C7 reaches 70 mol %, about 99% of the assembly is CW networks, suggesting that nearly all of the networks in the assembly are biased toward the preferential chirality of (S)-BIC-C7.

Interplay of the chiral coadsorber and the intrinsically chiral BIC-C7 analog

We next explored the interplay between the chiral coabsorber and the intrinsically chiral BIC-C7 analog at the liquid/solid interface. The chiral accordance situation was first studied, that is, chiral coabsorbers and the intrinsically stereogenic BIC-C7 derivatives with the same preferential handedness present in the molecular assembly simultaneously. It is found that CW networks are formed by codeposition of (S)-BIC-C7 and (S)-6O. Analogously, the coassembly of (R)-BIC-C7 and (R)-6O leads to CCW networks.

Then, chiral competition (that is, codeposition of the intrinsically chiral BIC-C7 derivatives with the 1-octanol derivative, which has an opposite chirality preference) was investigated. When (R)-BIC-C7 and (S)-6O were codeposited at the liquid/solid interface, global CW networks were observed. Typical STM images are shown in Fig. 5A. The structure of the (R)-BIC-C7/(S)-6O coassembly is identical to

the structures of the BIC-C7/1-octanol, BIC-C7/(S)-6O, and (R)-BIC-C7/1-octanol coassemblies. Figure 5B illustrates the formation of the (R)-BIC-C7/(S)-6O coassembly. The effect of the chiral coabsorber, that is, (S)-6O, predominates over that of the intrinsically chiral (S)-BIC-C7 and controls the chirality of the 2D molecular assembly. On the contrary, global CCW networks were formed by codeposition of (S)-BIC-C7 and (R)-6O. A typical STM image and the illustration of the formation of the (S)-BIC-C7/(R)-6O coassembly are shown in fig. S5. The chiral competition results indicate that the handedness of the 2D assembly is always consistent with the preferential handedness of the chiral coabsorber.

We further performed diluted chiral competition experiments between (R)-BIC-C7 and (S)-6O to evaluate their efficiency in chirality control. In all experiments in this section, the concentration of (R)-BIC-C7 was kept constant at 2.5×10^{-3} M, whereas the fraction of (S)-6O was varied using 1-octanol as an inert diluent. The black line in Fig. 5C shows the plot of the coverage of the CW honeycomb network in the monolayer versus the fraction of (S)-6O. When the fraction of (S)-6O is lower than 20 volume %, all domains in the monolayer are CCW. It is implied that the intrinsically chiral (R)-BIC-C7 controls the chirality of the 2D molecular assembly, and the effect of (S)-6O was not manifested. In the presence of about 30 volume % of (S)-6O in the solution, the CW network was observed in the
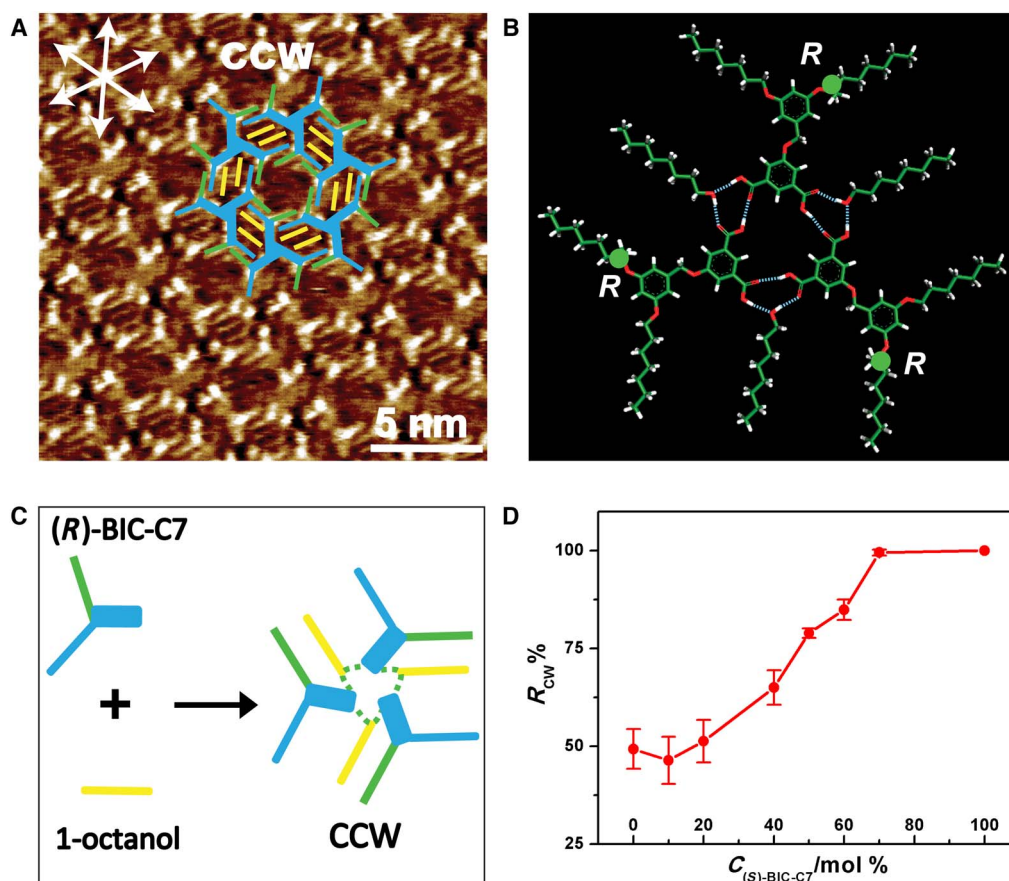
Fig. 4. Intrinsic molecular chirality induced the 2D molecular assembly. (A) High-resolution STM image of the (*R*)-BIC-C7/1-octanol assembly. I = 0.400 nA and V_{bias} = 0.900 V. (**B**) Calculated molecular model of the CCW trimer unit in the (*R*)-BIC-C7/1-octanol coassembly. The green dot marks the (*R*)-type chiral center in (*R*)-BIC-C7. (**C**) Formation of CCW trimer in the (*R*)-BIC-C7/1-octanol coassembly. The thick blue sticks, thin blue sticks, and green sticks represent the backbones, achiral side chains, and side chains with a chiral center of (*R*)-BIC-C7, respectively. The yellow sticks represent the coadsorbed 1-octanol molecules. (**D**) Plot of the coverage of the CW network in the ((*S*)-BIC-C7 + BIC-C7)/1-octanol assembly (R_{CW}, estimated based on the number of domains) versus the fraction of (*S*)-BIC-C7 (compared to the total content of BIC analogs) in the solution.

monolayer, as shown in fig. S6, except that the assembly is the same as that of the (*R*)-BIC-C7/1-octanol assembly, including the domain size, the angle between the neighboring domains, and the orientation of the assembly with respect to the substrate. When the fraction of (*S*)-6O in the solution reaches 50 volume % or higher, all networks in the monolayer are CW, and the CCW networks disappear. It means that the chiral coabsorber perfectly overwhelms the effect of the intrinsically chiral (*R*)-BIC-C7 and dominates the handedness of the molecular assembly. Diluted chiral competition experiments between (*S*)-BIC-C7 and (*R*)-6O give similar results. As shown by the red line in Fig. 5C, 50 volume % of (*R*)-6O in the solution is able to overrule the effect of the intrinsically chiral (*S*)-BIC-C7 and reverse the chirality of the 2D molecular assembly from CW to CCW.

We also investigated chiral competition between the chiral coabsorber and the intrinsically chiral BIC-C7 derivatives with two stereogenic centers, namely, (*S*,*S*)-BIC-C7 and (*R*,*R*)-BIC-C7. It is found that the CCW and CW networks are formed in the coassembly of (*R*,*R*)-BIC-C7/(*R*)-6O and (*S*,*S*)-BIC-C7/(*S*)-6O, respectively. The result is understandable because the codeposited 1-octanol derivative and the intrinsically chiral BIC-C7 derivative have the same chirality preference. When the chiral analog of 1-octanol and the intrinsically chiral BIC-C7 derivative with an opposite chirality preference, that is, (*R*,*R*)-BIC-C7

and (*S*)-6O, or (*S*,*S*)-BIC-C7 and (*R*)-6O, are codeposited on the surface, the 2D molecular assemblies formed show chirality preferred by the chiral coabsorber, as shown by the STM images in fig. S7. On the other hand, our attempt to investigate chiral competition between (*S*,*S*)-BIC-C7 [or (*R*,*R*)-BIC-C7] and (*S*)-BIC-C7 [or (*R*)-BIC-C7] in chirality control of the 2D molecular assembly failed because of molecular concentration–dependent polymorphism (*26*). (*S*,*S*)-BIC-C7 [or (*R*,*R*)-BIC-C7] forms the coassembled network BIC in 1-octanol only when the concentration is higher than 1×10^{-2} M, whereas BIC-C7 and (*S*)-BIC-C7 [or (*R*)-BIC-C7] form a quadrangular or lamellar structure instead of the coassembled network at a concentration that is higher than 2.5×10^{-3} M (*26*).

In addition, we explored the coassembly of (*S*)-4O and (*R*)-4O, that is, the chiral analog of 1-octanol with the methyl group attached to the fourth position, with the achiral and chiral BIC-C7 derivatives. CW and CCW networks were obtained for the BIC-C7/(*S*)-4O and BIC-C7/(*R*)-4O assemblies, respectively. When 20 volume % of (*S*)-4O was added to the 1-octanol solution of (*R*)-BIC-C7 [the concentration of (*R*)-BIC-C7 was kept constant at 2.5×10^{-3} M], the CW network, which is missed in the assembly of the (*R*)-BIC-C7/1-octanol assembly, appears in the monolayer, as shown in fig. S8. That means, (*S*)-4O, like (*S*)-6O, is able to induce the network with unfavored chirality of (*R*)-BIC-C7.
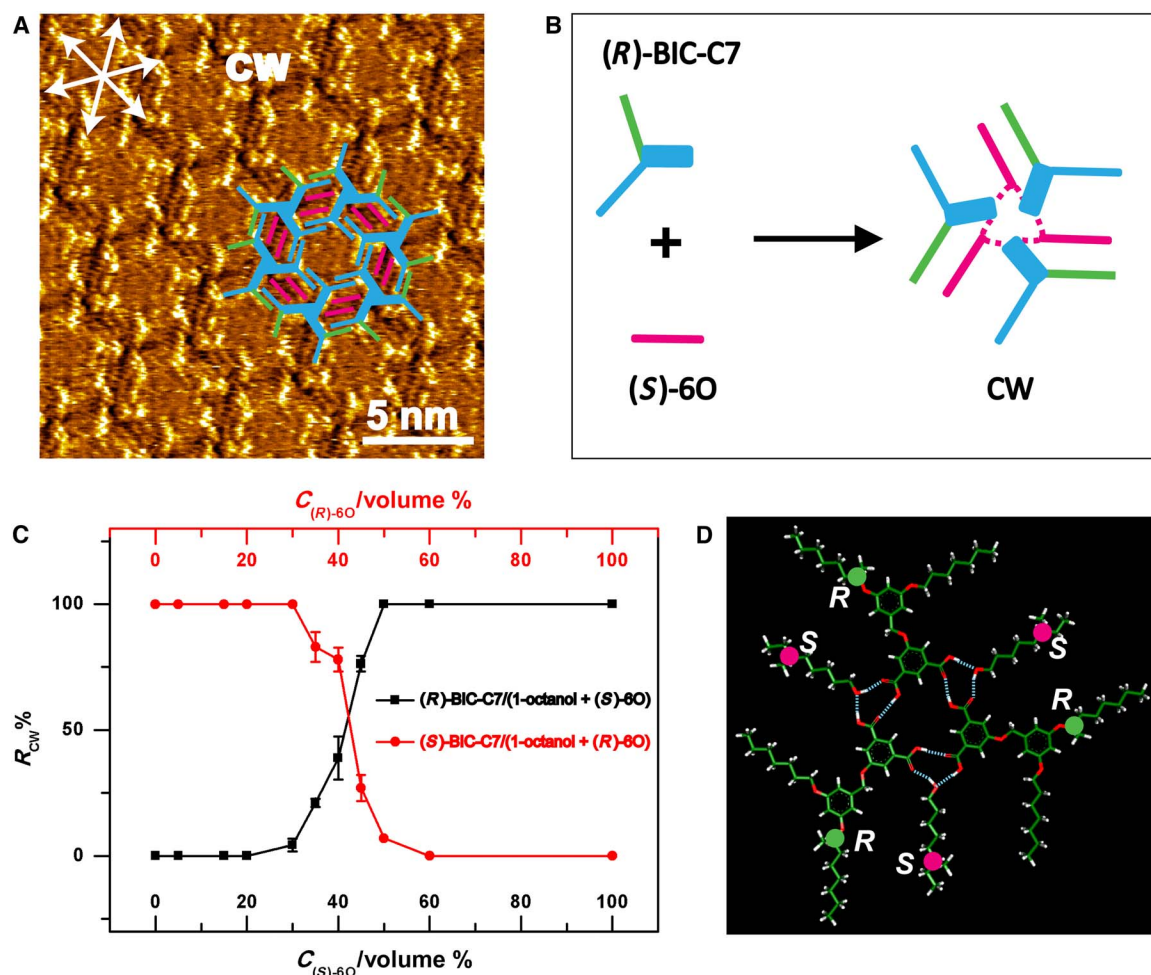
Fig. 5. Chiral competitive coassembly of (R)-BIC-C7 and (S)-6O. (**A**) High-resolution STM image of the CW network in the (R)-BIC-C7/(S)-6O coassembly. $I = 0.400$ nA and $V_{bias} =$ 0.900 V. (**B**) Formation of the CW trimeric unit in the (R)-BIC-C7/(S)-6O coassembly. The thick blue sticks, thin blue sticks, and green sticks represent the backbones, achiral side chains, and side chains with an (R)-type chiral center of (R)-BIC-C7, respectively. The red sticks represent the coadsorbed (S)-6O. (**C**) Plot of the coverage of the CW honeycomb network in the assembly (R_{CW}, estimated based on the number of domains) versus the fraction of (S)-6O (black line) or (R)-6O (red line) in the solution. (**D**) Calculated molecular model of the CW trimeric unit in the (R)-BIC-C7/(S)-6O assembly. The green and red dots mark the (R)-type and (S)-type chiral centers, respectively.

MM simulations

It is clear that both the chiral coadsorber and the intrinsically chiral BIC derivatives are able to induce a preferred chirality in the 2D molecular assembly of BIC analogs. To understand these phenomena, theoretical simulations were performed to reveal the difference in adsorption energy of the CW and CCW networks in the 2D molecular assembly.

The starting structural models used for theoretical simulations were built on the basis of STM images, in which the backbone of the BIC derivatives can be distinguished. Thus, the orientation of the backbones of the BIC derivative within a trimeric unit in the coassembly can be fixed, and the only flexible part is the side chain, which can rotate along the C–O bond. Therefore, for a trimeric unit in the coassembly of the BIC derivative and the 1-octanol analog, there are four adaptable adsorption conformations when confined on the surface. Figure S9 shows the four adaptable adsorption conformations of a trimeric unit in the BIC-C7/1-octanol coassembly. Correspondingly, four types of networks maybe formed, and they are used as the starting models for simulations of a coassembly.

The calculated molecular models for the BIC-C7/(S)-6O coassembly are shown in fig. S10. The adsorption energy of the trimeric unit (the

basic chiral unit of the 2D molecular assembly) of the energetically favored CW network is 4.89 kcal mol^{-1} (about 8 k_BT) higher than that of the energetically favored CCW network. This difference in adsorption energy could lead to obvious bias toward the CW network in the coassembly of BIC-C7 and (S)-6O. Similarly, the adsorption energy of the energetically favored CCW trimeric (R)-BIC-C7/1-octanol unit is 1.77 kcal mol^{-1} (about 3 k_BT) higher than that of the energetically favored CW trimeric (R)-BIC-C7/1-octanol unit, implying an efficient induction of CCW chirality in (R)-BIC-C7/1-octanol. The simulation results are consistent with the experimental results. Figure S11 shows the energetically favored CW and CCW networks of the (R)-BIC-C7/ 1-octanol coassembly.

MM simulations were performed on the (R)-BIC-C7/(S)-6O assembly to clarify the competitive induction of chirality preference. Both (R)-BIC-C7 and (S)-6O prefer to adsorb with the methyl group at the chiral center, pointing away from the surface for steric hindrance reason, as demonstrated in Figs. 3 and 4. When (R)-BIC-C7 and (S)-6O coassemble on the surface to form the honeycomb network, chiral centers within (R)-BIC-C7 and (S)-6O cannot adopt their preferential adsorption conformation at the same time because they have an

opposite chirality preference to the 2D molecular assembly. Either the methyl group at the chiral center in (S)-6O or that in (R)-BIC-C7 has to contact with the surface, corresponding to CCW network I or CW network II in fig. S12, respectively (optimized results). The energy of both molecular models increases significantly compared to that of the BIC-C7/1-octanol coassembly due to the steric hindrance effect induced by the methyl group pointing to the surface. To decrease the steric hindrance, the side chain with the attached chiral center in (R)-BIC-C7 was flipped 180° along the C–O bond so that both methyl groups in (R)-BIC-C7 and (S)-6O point away from the surface. Theoretical simulations indicate that the modified molecular model (network IV in fig. S12) is energetically favored compared with all the other surveyed structural models with different adsorption conformations of stereogenic centers. Figure 5D shows a trimeric unit of the energetically favored molecular model, revealing structural details. It can be seen that all methyl groups at the chiral centers point away from the surface to minimize the steric hindrance. The structural model is consistent with the experiment result, in which the CW network is preferred for the (R)-BIC-C7/(S)-6O assembly. Note that the energetically favored adsorption conformation of (R)-BIC-C7 in the (R)-BIC-C7/(S)-6O assembly is unfavored in the (R)-BIC-C7/1-octanol assembly (fig. S11). The CW network obtained in (R)-BIC-C7/(S)-6O is a compromised result, in which unfavored adsorption conformation is adopted to minimize the steric hindrance induced by the chiral center. On the other hand, the multiple hydrogen bonding between (R)-BIC-C7 and (S)-6O is relatively rigid, where slight variation of the hydroxyl or carboxyl groups may disturb the hydrogen bonding and interrupt the formation of the honeycomb networks. Consequently, the stereogenic information of the coadsorber can be efficiently transferred and dominate the chirality in the chiral competitive 2D molecular coassembly.

CONCLUSIONS

In conclusion, the interplay of noncovalently introduced chiral information with intrinsically molecular chirality in inducing 2D molecular chiral assembly was investigated. Both the intrinsically chiral molecule and the chiral coadsorber are able to induce global homochirality in the assembly of achiral analogs. Codeposition of the intrinsically chiral molecules and chiral coadsorbers results in 2D molecular assembly, with chirality preferred by the chiral coadsorber, suggesting that the chiral coadsorber can overrule the intrinsically molecular chirality and dominate the handedness of the molecular assembly. The steric hindrance that originated from the adsorption of the stereogenic center as well as the relatively rigid hydrogen bonding between the molecule and the coadsorber were suggested to be mainly responsible for the consequence. The results provide insights into the chirality induction in the molecular assembly on the surface and would benefit the development of highly efficient chirality control strategies.

MATERIALS AND METHODS
Preparation of the 2D molecular coassembly
To form the coassembly of the BIC derivative with 1-octanol or an analog of 1-octanol, the BIC derivative was dissolved in 1-octanol or the analog of 1-octanol to a final concentration of 2.5×10^{-3} M. Then, 1.0 μl of the solution was dropped onto a freshly cleaved HOPG (grade ZYB) surface to form the molecular assembly. In the chiral induction of the BIC-C7 assembly using (S)-6O as the chiral seed, BIC-C7 was dissolved in a mixed solution of 1-octanol and (S)-6O. The concentration of BIC-

C7 was constant at 2.5×10^{-3} M, and the fraction of (S)-6O in the mixed solution varies. In the chiral induction of BIC-C7 using (S)-BIC-C7 as chiral seeds, BIC-C7 and (S)-BIC-C7 were dissolved in 1-octanol together. The total content of the BIC analog was kept constant at 2.5×10^{-3} M, but the ratio of BIC-C7 to (S)-BIC-C7 was varied. In the diluted chiral competition experiments between (R)-BIC-C7 and (S)-6O, the concentration of (R)-BIC-C7 was kept constant at 2.5×10^{-3} M, whereas the fraction of (S)-6O was varied using 1-octanol as an inert diluent. Note that to form the network of (R,R)-BIC-C7 or (S,S)-BIC-C7, the concentration of (R,R)-BIC-C7 or (S,S)-BIC-C7 should be 0.01 M.

STM measurements and statistical analysis
STM measurements were performed at room temperature (298 K) at the liquid/solid interface directly using PicoSPM (Agilent Technologies) with a mechanically cutting Pt/Ir wire (90:10) as the tip. All STM images were recorded in constant current mode and shown without any image processing.

For statistical analysis, we first prepared several parallel molecular solutions (the compositions of the parallel solutions are the same in theory); then, 0.5 μl of each parallel solution was deposited on a freshly cleaved HOPG surface to obtain a sample, as named in this study, with molecular adlayers at the liquid/solid interface. Typically, five parallel solutions or five samples on different HOPG substrates were prepared unless otherwise specified. To estimate the coverage of the CW or CCW network in a sample, we recorded about 50 STM images (100 nm × 100 nm) with more than four domains in each image at different locations of the adlayer. The total number of CW and CCW domains in these STM images was counted, and the coverage of the CW or CCW network (denoted as R_{cw} and R_{ccw}, respectively) was calculated according to the following formula: $R_{cw} = N_{cw}/(N_{cw} + N_{ccw})$, $R_{ccw} = N_{ccw}/(N_{cw} + N_{ccw})$, where N_{cw} and N_{ccw} are the total number of the CW and CCW domains in a sample. Note that the coverage values shown in this study are average values of these parallel samples, and the error bar is an SD that is estimated according to the following formula: $\sigma = \sqrt{\frac{1}{n-1}\sum_{i=1}^{n}(R_{CW,i} - \overline{R_{CW}})}$, where σ refers to the SD, n is the number of parallel samples, $R_{CW,i}$ is the calculated coverage of the CW network in a sample, and $\overline{R_{CW}}$ is the average coverage of the CW networks for the parallel samples.

Theoretical simulations
A hexagonal unit of the network that is built on the basis of the STM images was used as the initial molecular model of MM simulations. Three graphene layers were used as the substrate and fixed during the geometry optimization. The geometry optimization of molecular adlayers was performed by MM simulations using the Dreiding force field until convergence criteria of gradient energy and force residue larger than 2×10^{-5} kcal mol^{-1} and 0.001 kcal mol^{-1} Å^{-1}, respectively, were reached. The energy given in the present study is the total energy of the optimized unit.

SUPPLEMENTARY MATERIALS

fig. S6. Typical STM image of the assembly when (R)-BIC-C7, 1-octanol, and (S)-6O are codeposited together.

fig. S7. Chiral competition between chiral coabsorber and (R,R)-BIC-C7 [or (S,S)-BIC-C7].

fig. S8. Coassembly of (R)-BIC-C7 and 1-octanol before and after the presence of (S)-4O.

fig. S9. Adaptable adsorption conformation of a trimeric unit in the BIC-C7/1-octanol coassembly.

fig. S10. Calculated hexagonal units of the networks in the BIC-C7/(S)-6O coassembly.

fig. S11. Calculated hexagonal units of the networks in the (R)-BIC-C7/1-octanol coassembly.

fig. S12. Calculated hexagonal units of the networks in the (R)-BIC-C7/(S)-6O coassembly.

REFERENCES AND NOTES

1. M. Linares, A. Minoia, P. Brocorens, D. Beljonne, R. Lazzaroni, Expression of chirality in molecular layers at surfaces: Insights from modelling. *Chem. Soc. Rev.* **38**, 806–816 (2009).

2. R. Raval, Chiral expression from molecular assemblies at metal surfaces: Insights from surface science techniques. *Chem. Soc. Rev.* **38**, 707–721 (2009).

3. W. D. Xiao, K.-H. Ernst, K. Palotas, Y. Zhang, E. Bruyer, L. Peng, T. Greber, W. A. Hofer, L. T. Scott, R. Fasel, Microscopic origin of chiral shape induction in achiral crystals. *Nat. Chem.* **8**, 326–330 (2016).

4. S. Haq, N. Liu, V. Humblot, A. P. J. Jansen, R. Raval, Drastic symmetry breaking in supramolecular organization of enantiomerically unbalanced monolayers at surfaces. *Nat. Chem.* **1**, 409–414 (2009).

5. F. García, L. Sánchez, Structural rules for the chiral supramolecular organization of OPE-based discotics: Induction of helicity and amplification of chirality. *J. Am. Chem. Soc.* **134**, 734–742 (2012).

6. A. J. Therrien, T. J. Lawton, B. Mernoff, F. R. Lucci, V. V. Pushkarev, A. J. Gellman, E. C. H. Sykes, Chiral nanoscale pores created during the surface explosion of tartaric acid on Cu(111). *Chem. Commun.* **52**, 14282–14285 (2016).

7. M. Parschau, S. Romer, K.-H. Ernst, Induction of homochirality in achiral enantiomorphous monolayers. *J. Am. Chem. Soc.* **126**, 15398–15399 (2004).

8. Y. Yun, A. J. Gellman, Adsorption-induced auto-amplification of enantiomeric excess on an achiral surface. *Nat. Chem.* **7**, 520–525 (2015).

9. R. Fasel, M. Parschau, K.-H. Ernst, Amplification of chirality in two-dimensional enantiomorphous lattices. *Nature* **439**, 449–452 (2006).

10. K. Tahara, H. Yamaga, E. Ghijsens, K. Inukai, J. Adisoejoso, M. O. Blunt, S. De Feyter, Y. Tobe, Control and induction of surface-confined homochiral porous molecular networks. *Nat. Chem.* **3**, 714–719 (2011).

11. F. Masini, N. Kalashnyk, M. M. Knudsen, J. R. Cramer, E. Lægsgaard, F. Besenbacher, K. V. Gothelf, T. R. Linderoth, Chiral induction by seeding surface assemblies of chiral switches. *J. Am. Chem. Soc.* **133**, 13910–13913 (2011).

12. A. Nuermaimaiti, C. Bombis, M. M. Knudsen, J. R. Cramer, E. Lægsgaard, F. Besenbacher, K. V. Gothelf, T. R. Linderoth, Chiral induction with chiral conformational switches in the limit of low "sergeants to soldiers" Ratio. *ACS Nano* **8**, 8074–8081 (2014).

13. M. M. Green, M. P. Reidy, R. D. Johnson, G. Darling, D. J. O'Leary, G. Willson, Macromolecular stereochemistry: The out-of-proportion influence of optically active comonomers on the conformational characteristics of polyisocyanates. The sergeants and soldiers experiment. *J. Am. Chem. Soc.* **111**, 6452–6454 (1989).

14. T. Kim, T. Mori, T. Aida, D. Miyajima, Dynamic propeller conformation for the unprecedentedly high degree of chiral amplification of supramolecular helices. *Chem. Sci.* **7**, 6689–6694 (2016).

15. M. M. Green, B. A. Garetz, B. Munoz, H. P. Chang, S. Hoke, R. Graham Cooks, Majority rules in the copolymerization of mirror-image isomers. *J. Am. Chem. Soc.* **117**, 4181–4182 (1995).

16. E. Yashima, N. Ousaka, D. Taura, K. Shimomura, T. Ikai, K. Maeda, Supramolecular helical systems: Helical assemblies of small molecules, foldamers, and polymers with chiral amplification and their functions. *Chem. Rev.* **116**, 13752–13990 (2016).

17. J. Seibel, O. Allemann, J. S. Siegel, K.-H. Ernst, Chiral conflict among different helicenes suppresses formation of one enantiomorph in 2D crystallization. *J. Am. Chem. Soc.* **135**, 7434–7437 (2013).

18. C. Roth, D. Passerone, K.-H. Ernst, Pasteur's quasiracemates in 2D: Chiral conflict between structurally different enantiomers induces single-handed enantiomorphism. *Chem. Commun.* **46**, 8645–8647 (2010).

19. S. J. George, Ž. Tomović, A. P. H. J. Schenning, E. W. Meijer, Insight into the chiral induction in supramolecular stacks through preferential chiral solvation. *Chem. Commun.* **47**, 3451–3453 (2011).

20. S. J. George, Ž. Tomović, M. M. J. Smulders, T. F. A. de Greef, P. E. L. G. Leclère, E. W. Meijer, A. P. H. J. Schenning, Helicity induction and amplification in an oligo(p-phenylenevinylene) assembly through hydrogen-bonded chiral acids. *Angew. Chem. Int. Ed.* **46**, 8206–8211 (2007).

21. I. Destoop, H. Xu, C. Oliveras-González, E. Ghijsens, D. B. Amabilino, S. De Feyter, 'Sergeants-and-Corporals' principle in chiral induction at an interface. *Chem. Commun.* **49**, 7477–7479 (2013).

22. T. Chen, W.-H. Yang, D. Wang, L.-J. Wan, Globally homochiral assembly of two-dimensional molecular networks triggered by co-absorbers. *Nat. Commun.* **4**, 1389 (2013).

23. T. Chen, S.-Y. Li, D. Wang, M. Yao, L.-J. Wan, Remote chiral communication in coadsorber-induced enantioselective 2D supramolecular assembly at a liquid/solid interface. *Angew. Chem. Int. Ed.* **54**, 4309–4314 (2015).

24. S. Sforza, T. Tedeschi, R. Corradini, R. Marchelli, Induction of helical handedness and DNA binding properties of peptide nucleic acids (PNAs) with two stereogenic centres. *Eur. J. Org. Chem.* **2007**, 5879–5885 (2007).

25. K. Tang, M. M. Green, K. S. Cheon, J. V. Selinger, B. A. Garetz, Chiral conflict. The effect of temperature on the helical sense of a polymer controlled by the competition between structurally different enantiomers: From dilute solution to the lyotropic liquid crystal state. *J. Am. Chem. Soc.* **125**, 7313–7323 (2003).

26. X. Zhang, T. Chen, Q. Chen, G.-J. Deng, Q.-H. Fan, L.-J. Wan, One solvent induces a series of structural transitions in monodendron molecular self-assembly from lamellar to quadrangular to hexagonal. *Chemistry* **15**, 9669–9673 (2009).

Citation: T. Chen, S.-Y. Li, D. Wang, L.-J. Wan, Competitive chiral induction in a 2D molecular assembly: Intrinsic chirality versus coadsorber-induced chirality. *Sci. Adv.* **3**, e1701208 (2017).